Modulation of BK channel voltage gating by different auxiliary β subunits

Gustavo F. Contreras[a,b], Alan Neely[a], Osvaldo Alvarez[a,c], Carlos Gonzalez[a,1], and Ramon Latorre[a,1]

[a]Centro Interdisciplinario de Neurociencia de Valparaíso, Facultad de Ciencias, and [b]Doctorado en Ciencias mención Neurociencia, Universidad de Valparaíso, Valparaíso 2366103, Chile; and [c]Facultad de Ciencias, Universidad de Chile, Santiago 7800003, Chile

Contributed by Ramon Latorre, October 1, 2012 (sent for review September 5, 2012)

Calcium- and voltage-activated potassium channels (BK) are regulated by a multiplicity of signals. The prevailing view is that different BK gating mechanisms converge to determine channel opening and that these gating mechanisms are allosterically coupled. In most instances the pore forming α subunit of BK is associated with one of four alternative β subunits that appear to target specific gating mechanisms to regulate the channel activity. In particular, β1 stabilizes the active configuration of the BK voltage sensor having a large effect on BK Ca^{2+} sensitivity. To determine the extent to which β subunits regulate the BK voltage sensor, we measured gating currents induced by the pore-forming BK α subunit alone and with the different β subunits expressed in *Xenopus* oocytes (β1, β2IR, β3b, and β4). We found that β1, β2, and β4 stabilize the BK voltage sensor in the active conformation. β3 has no effect on voltage sensor equilibrium. In addition, β4 decreases the apparent number of charges per voltage sensor. The decrease in the charge associated with the voltage sensor in α β4 channels explains most of their biophysical properties. For channels composed of the α subunit alone, gating charge increases slowly with pulse duration as expected if a significant fraction of this charge develops with a time course comparable to that of K^+ current activation. In the presence of β1, β2, and β4 this slow component develops in advance of and much more rapidly than ion current activation, suggesting that BK channel opening proceeds in two steps.

kinetic model | modulatory beta subunits

The open probability of large conductance Ca^{2+}- and voltage-activated K^+ (BK) channels increases when confronted with a membrane depolarization or an increase in the intracellular Ca^{2+} concentration (1–3). The BK pore-forming α subunit is coded by a single gene (*Slo1; KCNMA1*) and yet, it displays a variety of phenotypes in different cells and tissues as a consequence of alternative splicing, metabolic regulation, and modulation by β subunits. This great diversity of BK channels is fundamental to the adequate function of many tissues. In particular, β subunits are associated with BK channels in most tissues where they are present and dramatically modify their gating properties (4).

At present, four β subunits have been cloned in mammals (β1–β4) (4–10). BK β subunits have two transmembrane segments joined together by a loop (~148-aa residues). The external loop, and N and C termini are intracellular. Sequence similarities are major between β1–β2 and β2–β3, respectively. β4 is the most distantly related of all β subunits. β1 and β2 subunits induce an increase of the apparent Ca^{2+} sensitivity and a slowing of the macroscopic kinetics (4, 7, 8). β2 also induces fast and complete inactivation (6, 10, 11) and an instantaneous outward rectification that suggests that the β2 external loop approaches the BK pore as to alter ion conduction (12). Four splice variants of β3 have been identified, β3a–c. β3b induces fast and partial inactivation of BK currents and also produces an outward rectification of the open channel currents (10, 13). Outward rectification is regulated by the extracellular segment of this subunit (14). β4 has a complex Ca^{2+} concentration-dependent effect on BK channel gating. This subunit decreases apparent Ca^{2+} sensitivity at low Ca^{2+} concentrations but induces an increase in the apparent sensitivity at high Ca^{2+} concentrations (8, 14–18). β4 also slows down activation and deactivation kinetics (7, 8).

Despite the fact that the BK phenotype produced by each of the β subunits has been well characterized, controversies exist regarding the biophysical mechanisms by means of which these auxiliary subunits modify BK channel gating (19–23). Since the finding of Bao and Cox (19) that the main effect of the β1 subunit is to alter the equilibrium between the resting and active configurations of the voltage sensor, several important questions remain to be answered: To what extent do β2 and β4 alter BK channel voltage sensing? Does the slow component of the OFF gating charge detected by Horrigan et al. (24) in channels formed by the α subunit alone parallel the slowing down in the I_K activation induced by β1, β2, and β4 as predicted by the two-tiered allosteric model? To assay potential effects of the β subunits on the workings of the voltage sensor, we measured gating currents (I_g) induced by channels formed by the pore-forming BK α subunit alone and with the different β subunits expressed on *Xenopus* oocytes (β1, β2IR, β3b, and β4).

Results

Characterization of BK Gating Currents in the Presence of β Subunits. We first measured the macroscopic K^+ currents (I_K) in the cell-attached configuration to confirm that BK channels were formed by the expected α or α/β complex (Fig. S1). In cell-attached configuration the large size of the ionic currents prevented adequate voltage clamp. Therefore, we lowered K^+ to record current in symmetrical 1-mM K^+ (Fig. 1, *Left*) in excised patches. Notice in Fig. 1 *B*, *C*, and *E* that the time course of the K^+ currents of channels formed by α/β1, α/β2, and α/β4 were much slower than the ones of channels formed by the α subunit alone (Fig. 1*A*). The slowing of the K^+ current by coexpression of the these β subunits is one of the hallmarks of the phenotype of channels formed by α/β*x* (*x* = 1,2,4). For β3, (α/β3) BK channels were identified by a small, fast, and incomplete inactivation process (Fig. 1*D*).

After patch excision, I_g currents were measured in conditions of 0 K^+ and 0 Ca^{2+} by profusely perfusing the internal side of the macropatch with a K^+-free solution (Fig. 1, *Right*). Gating current recordings reveal fast time courses with time constants, which were not very different between the different subunit combinations. In addition, the gating currents develop fully before channel opening (e.g., Fig. S1). These results show that in BK channels voltage sensor activation occurs before channel opening, as previously reported for the cases of α and α/β1 BK channels (19, 25, 26). In other words, in the absence of Ca^{2+}, BK gating charge movement takes place between several closed states.

Families of I_g as those shown in Fig. 1, *Right* evoked at different voltages (−90 to 350 mV) were integrated between the beginning and the end of the pulse to obtain the gating charge activation relationships, Q_{ON}–V and Q_{OFF}–V. For all of the different types of channels tested and for voltage pulses of 1 ms in

Author contributions: G.F.C., A.N., C.G., and R.L. designed research; G.F.C. and C.G. performed research; G.F.C., A.N., O.A., C.G., and R.L. analyzed data; and O.A., C.G., and R.L. wrote the paper.

The authors declare no conflict of interest.

[1]To whom correspondence may be addressed. E-mail: ramon.latorre@uv.cl or carlos.gonzalezl@uv.cl.

This article contains supporting information online at www.pnas.org/lookup/suppl/doi:10.1073/pnas.1216953109/-/DCSupplemental.

PHYSIOLOGY

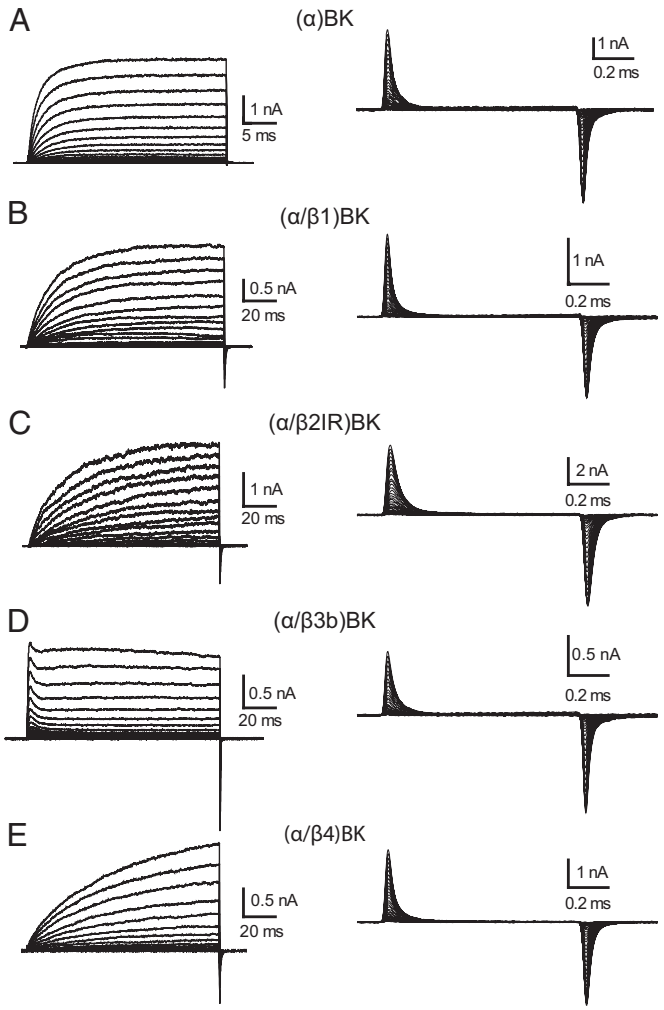

Fig. 1. Ionic and gating currents for (α)BK and (α/βx)BK channels. (*A–E*, *Left*) Representative families of I_K evoked by voltage steps of 50 ms for (α)BK and 120 ms for the α/β*x* complexes, going from 0 to 250 mV in 10-mV steps. Ionic currents were recorded in 1-mM symmetrical K^+ and ~5 nM Ca^{2+}. (*A–E*, *Right*) Gating currents elicited by 1-ms steps to increasing voltages from −90 to 350 mV in increments of 10 mV; pulse duration was set to reach a quasi steady state.

duration, all of the ON charge was recovered in the OFF charge (Fig. S2). As shown in Fig. 1, *Right*, I_g time courses recorded from the different channels were similar despite the fact that I_K time courses are widely different between channels formed by α and α/β*x* (x = 1,2,4). *Q–V* relationships for each channel type were fitted with Boltzmann functions and normalized to their maxima and averaged to yield the *Q–V* curves shown in Fig. 2 *A–D*. Compared with (α)BK channels (gray symbols), coexpression with β1 and β2 shifts the *Q–V* curves along the voltage axis to the left by 57 and 39 mV, respectively, with no appreciable changes in the voltage dependency of activation, z (Fig. 2 *A*, *B*, *E*, and *F*). The values of $V_{1/2}$ and z for (α)BK, (α/β1)BK channels (Fig. 2 *E* and *F*) are in reasonable agreement with those previously reported (19, 25, 27). Coexpression with β4 subunits, on the other hand, produced a 22-mV right shift of the $V_{1/2}$ of the *Q–V* curve and a 23% decrease in z (Fig. 2 *D* and *F*). Calculation of the standard free energy difference (ΔG^0) between the active and resting states of the voltage sensor at Vm = 0, $\Delta G^0 = zFVo$, reveals that β1, β2IR, and β4 subunits stabilize the active state of the sensor. For α subunit alone, ΔG^0 is 10.3 kJ/mol; this energy drops to 6.3, 7.7, and 8.6 kJ/mol when BK is coexpressed with β1, β2IR, and β4 subunits, respectively. These results show that not only β1, but also β2IR and β4 stabilize the voltage sensor in its active configuration at 0 mV. β3b has no effect on ΔG^0 (Fig. 2 *C* and *E*).

β Subunits and the Slow Gating Charge Recovery. The lack of a rising phase, the exponential decay of I_g, and the fact that the *Q–V* relationship was well described by a single Boltzmann function are indicative of a two-state model in the case of (α)BK channels, one resting and one active, and is adequate to describe the early movement of the voltage sensor (Fig. 2) (25). This voltage sensor behavior was conserved in the presence of the different β subunits (Table S2). First, we found that the exponential decay of I_g and the Q_{ON}–V relationships are well described by a single time constant (τ) (Fig. S3) and single Boltzmann function, irrespective of the β subunit present (Fig. 2 *B–D*) and second, in all cases, the τ(V) (Fig. S4) was well described by:

$$\tau(V) = \frac{1}{\alpha(V) + \beta(V)}, \qquad [1]$$

where $\alpha(V) = \alpha_0 \exp(z\delta e_0 V/kT)$ is the forward rate constant and $\beta(V) = \beta_0 \exp(z(\delta - 1)e_0 V/kT)$ is the backward rate constant, which determine the equilibrium constant, J, which characterizes the resting–active transition of the voltage sensor, i.e., $J(V) = \alpha(V)/\beta(V)$ (Fig. S5). The parameter z is the number of effective

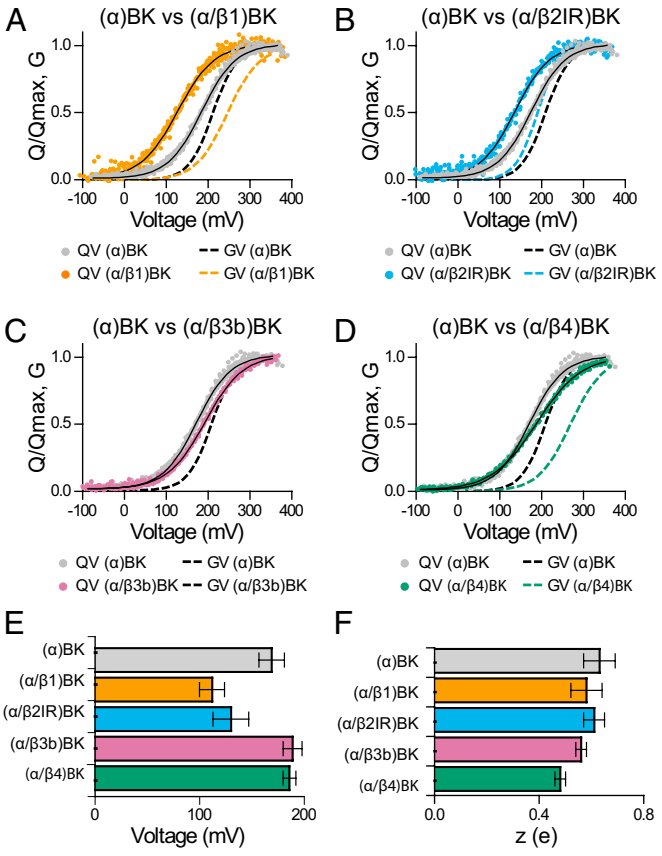

Fig. 2. Gating charge–voltage relationships for (α)BK and (α/βx)BK channels. (*A–D*) *Q–V* and *G–V* relations for the indicated (α)BK and (α/βx)BK complexes. For comparison, all *Q–V* graphs include the *Q–V* curve from channels formed by the α subunit alone (gray circles). They also include *G–V* curves from ref. 33 for (α)BK (dashed black line), (α/β1)BK (dashed orange line), and (α/β2IR)BK (dashed sky-blue line). The *G–V* for (α/β4)BK channels (dashed bluish-green line) was from ref. 31). The data from many experiments (n = 7–14) were aligned by shifting them along the voltage axis by the mean $\Delta V_{1/2} = (<V_{1/2}> - V_{1/2})$, and fitted by Boltzmann function. (*E* and *F*) Quantification of $V_{1/2}$ and z obtained from fits to the *Q–V* relations (mean ± SD; Table S1).

charges displaced during the transitions, and δ is the electrical distance at which the peak of the energy barrier that separates the resting and active states of the sensor is located. As expected from the $V_{1/2}$ of the Q–V curves, the peaks of the $\tau(V)$ curves for (α/β1)BK and (α/β2)BK obtained from the fit to the $\tau(V)$ data to Eq. **1** were leftward shifted compared with (α)BK channels by 50 and 30 mV, respectively (Fig. S4 *B* and *C* and Table S1). The value obtained for δ indicates that the energy barrier that separates resting and active states of the voltage sensor is highly asymmetric and that most of the voltage dependence resides in the rate constant β. The behavior of the voltage sensor of (α/β4)BK channels is also well explained using a two-state model. However, the large difference in the voltage at which we found $\tau(V)_{peak}$ and the $V_{1/2}$ for the $Q(V)$ is a consequence of the decrease in z promoted by this subunit.

Fig. 3*A* shows the different voltage pulse protocols used to determine the different kinetic components of the gating currents. The existence of a slow component of charge movement was detected as an increase in the Q_{OFF} after voltage pulses of increasing duration (25, 27). The origin of this slow component has been explained in terms of an allosteric voltage-gating scheme (25) (Fig. S5*A*). This model predicts that this slow off-gating charge develops with a time constant that matches the time constant of the ionic current activation. Fig. 3*B* shows that for (α)BK channels, as predicted by the allosteric model, the relative contribution of the slow component of Q_{OFF} augments as the voltage of the test pulse is increased. This is a clear indication of the existence of additional slow components in I_{gON} whose amplitudes are too small to be detected during the ON pulse, but which can be detected during repolarization because charge returns at a faster rate. The amount of Q_{OFF} as a function of pulse duration is well described by a double exponential function (Fig. 3*B*, solid line). The time constant for the slow component (Fig. 3*C*, open circles), as predicted by the Horrigan et al. (24) model, is similar to the time constant that describes ionic current activation (data from ref. 20 and gray circles). In contrast to (α)BK channels, the slower components of the gating charge for (α/β1)BK, (α/β2IR)BK, and (α/β4)BK channels appear at lower voltages (Fig. 4 *D*, *F*, and *J*), and they are almost absent in the case of (α/β2IR)BK channels (Fig. 3*F*). In addition, this slow component is observed at voltages at which channels do not open. This can be better appreciated in the behavior of the amplitude of the slow component (A_{slow} in Fig. 3 *E*, *G*, and *K*). For (α/β1)BK, (α/β2IR)BK, and (α/β4)BK channels, the amplitude of A_{slow} is large, even at very low open probabilities. Moreover, for these channels, the time constant of the slow Q_{OFF} is between 10 and 30 times faster than for I_K activation (Fig. 4 *E*, *G*, and *K*). The two-tiered allosteric model on Fig. S5*A* cannot explain these experimental results (*SI Materials and Methods*).

It can be argued that differences in τ_{Qslow} and $\tau_{activation}$ are due to differences in the experimental conditions at which these two sets of experiments were obtained. In particular, it is possible that the ionic composition of the solutions became important in determining the speed at which the gating and the ionic currents develop. To test for this possibility, we measured the ionic current activation time constants at 1 mM symmetrical K^+, an ionic milieu that is closer to the one used to measure gating currents (Fig. 4, colored circles), and found that $\tau_{activation}$ is similar to the $\tau_{activation}$ obtained in 100 mM symmetrical (e.g., colored circles with solid line in Fig. 3 *C*, *E*, and *G*).

Taking into account that the Horrigan–Cui–Aldrich model (H–C–A) (24) (Fig. S5*A*) demands that the time constant of the slow Q_{OFF} should follow a time course comparable to that of channel opening, we reasoned that in the presence of the β1 and β2 subunits the slow Q_{OFF} actually represents charge moving between closed states. Under this assumption, we found that an extension of the H–C–A allosteric model that includes an extra row of intermediate closed ($C_{1,i}$) states suffices to explain our results. In this version of the model, the time constant of Q_{OFF} slow need not be equal to the time constant of ionic current activation (Fig. 4 and Fig. S5*B*). We hypothesize that in the presence of β1 and β2 subunits there is an increase in the energy barrier connecting the intermediate closed states with the open states. In this case, the slow component of Q_{OFF} reflects $C_{0,i}$ to $C_{1,i}$ ($i = 0, 1..,4$) transitions plus the relaxation of the equilibrium distribution among the $C_{1,i}$ states. Considering that transitions from the intermediate closed to the open states are very slow, these processes will generate no detectable gating currents because of their small amplitudes and long time constants. In addition, our model does not predict the presence of flickers inside a burst, which are evident in the single channel measurements (28). Therefore, we think that flickers should arise from transitions from the open state to yet another closed state that is not part of the present model. With this extended allosteric model, it is possible to conclude that β1 and β2 subunits shift the Q–V curve to the left along the voltage axis by modifying the equilibrium that defines the resting–active voltage sensor reaction. The slowing of both activation and deactivation kinetics of the macroscopic currents is most economically explained by an increase in the energy barrier connecting the intermediate closed states to the open states. This is a large departure from previous proposed models to explain BK gating in the presence of β subunits and implies that BK channel opening is more complex than previously thought. We have performed a global fit to the data obtained using (α/β1)BK channels (Fig. 4). The model matches the data reasonably well and in particular accounts for the kinetic and equilibrium behavior of Q_{slow}.

Discussion

Although the apparent Ca^{2+} sensitivity of BK channels is increased and the gating kinetics slowed down by both the β1 and β2 subunits, several reports indicate that these subunits enhance channel activity through different molecular mechanisms (20, 21, 29). However, the fluorescence studies of Savalli et al. (30) indicate that similarly to β1 (19), β2 coexpression stabilizes the active state of the voltage sensor, consequently increasing the apparent Ca^{2+} sensitivity of the channel. Even for the β1 subunit there still disagreements in the literature whether or not this subunit acts purely by modifying voltage sensor activation or also affects Ca^{2+} sensitivity of the BK channel (21, 22).

Early work suggested that the enhancement of the BK channel's Ca^{2+} sensitivity mediated by the β1 subunit is due to effects unrelated to Ca^{2+} binding (28, 31). β1 is able to increase burst duration in the absence of Ca^{2+} an effect that produces a 10-fold increase in the open probability (P_o). This increase may explain most of the leftward shift of the P_o vs. Ca^{2+} relationship (28). On the other hand, the allosteric model predicts that β1 increases the Ca^{2+} sensitivity mainly by altering aspects of gating that do not involve Ca^{2+} binding but it also demands albeit small, significant modifications to the channel Ca^{2+} binding affinity (31). This and subsequent studies have suggested that β1 modifies the apparent Ca^{2+} sensitivity by altering voltage-dependent gating (16, 19, 20, 31). In this regard, it is noteworthy that β1 is able to partially restore the BK channel Ca^{2+} sensitivity of a mutant in which the Ca^{2+} sensitivity has been obliterated by neutralizing the aspartates contained in the Ca^{2+} bowl and those of the second high-affinity Ca^{2+} site present in the RCK1 domain (32). These results suggest that rather than acting directly on the Ca^{2+} binding sites, β1 modulates the allosteric coupling between the Ca^{2+} binding sites and the gate. Among the wide range of effects induced by β1, the most dramatic one is the −57-mV leftward shift of the Q–V relationship of the (α/β1)BK relative to the $V_{1/2}$ obtained from (α)BK channels (Fig. 2*A*). This shift implies a stabilization of the active configuration of the voltage sensor and is consistent with the idea that the work that Ca^{2+} binding must do to open the channel is decreased. The net effect is an apparent enhancement of the Ca^{2+} sensitivity. Actually, changes in the equilibrium that govern the transition between resting and active configuration of the voltage sensor account for the majority of the effects of β1. Some reports indicate, however, that it is necessary to invoke changes in the true Ca^{2+} affinity to account fully for the effects of this subunit on Ca^{2+} sensitivity (19, 22, 31). This conclusion is in conflict with the results of Yang et al.

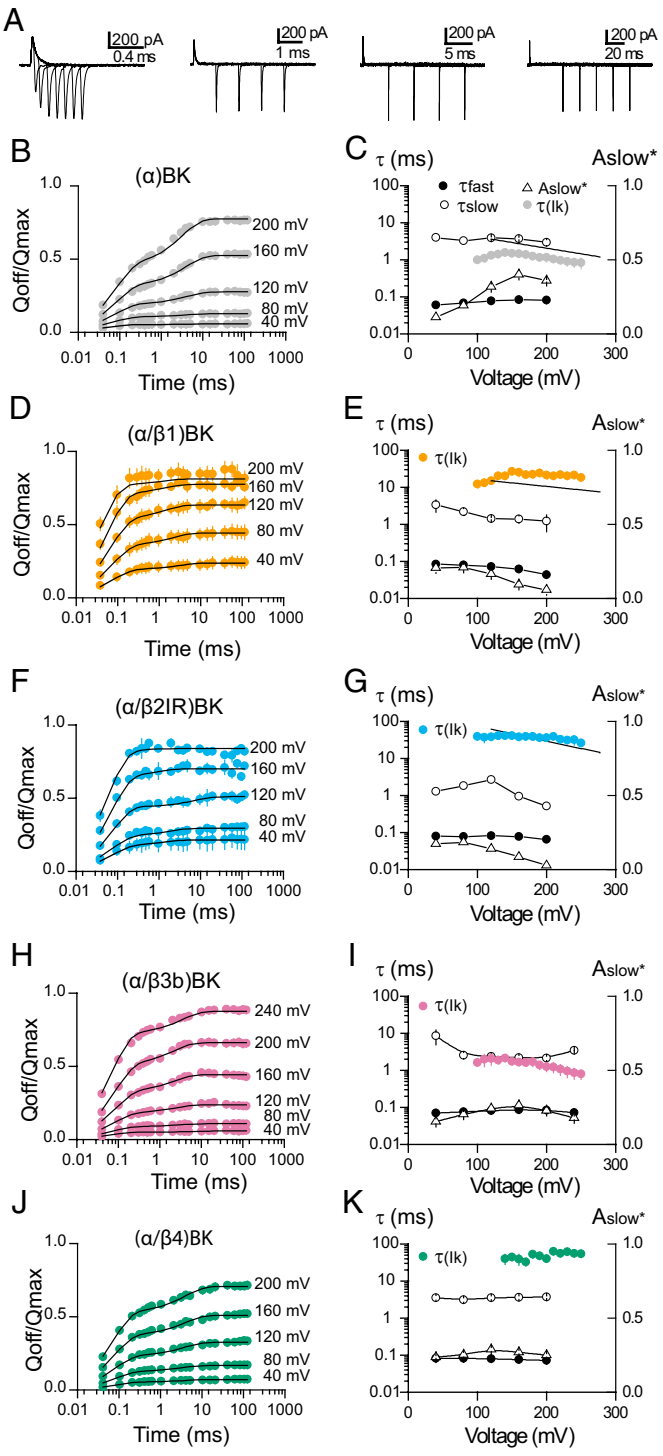

Fig. 3. Slow gating charge kinetics. (*A*) Representative recordings of gating currents evoked by 200-mV pulses with different durations from 0.04 to 120 ms. Each family of I_g was recorded with different voltage pulse protocol at the same voltage. (*B, D, F, H,* and *J*) OFF charge as function of voltage pulse duration for (α)BK and (α/βx)BK (x =1–4) channels. The OFF charge (Q_{OFF}; filled circles, mean ± SEM) was integrated in a range of 1 ms, normalized to the Q_{MAX} for each patch, and plotted against the pulse duration (time; logarithmic scale) for different voltage steps (40, 80, 120, 160, and 200 mV). The Q_{OFF} vs. t relation was fitted with a two-component exponential function (solid line) with time constant an amplitude of the fast component constrained to the exponential fit of I_{gON} at these voltages. (*C, E, G, I,* and *K*) Parameters defining the fast and slow components as a function of voltage for (α)BK and (α/βx)BK (x = 1–4) channels. For comparison the time constants of the I_K activation (τ_{Ik}, filled colored circles) are also shown. Time constants of the fast components of I_g (τ_{fast}) are represented by the open circles and the time constants of the slow components (τ_{slow}) are represented by the filled circles; A_{slow}* is the fractional amplitude of the slow components (A_{slow}* = A_{slow}/(A_{fast} + A_{slow}), open triangles), and *C* and *E–G* include the fits over the linear range of the I_K activation time constant reported by Orio and Latorre (20); solid black lines.

(21), who reported that neutralization of the BK voltage sensing residues abolished the leftward shift induced by β1.

Surprisingly, β1 does not affect gating current kinetics, suggesting that the slowing of BK channel activation and deactivation kinetics is a process related to the transition between closed and open states. In the present study, by applying prolonged depolarizations we were able to determine directly the effects of β1 on the charge movement between closed estates. Our results indicate that β1, β2IR, and β4 profoundly affect both the amplitude and the kinetics of the slow gating component (Fig. 3 *E*, *G*, and *K*), an observation that we have interpreted using the model depicted in Fig. 4*A*. This model is able to account for the data presented here and indicates that β1 and β2 stabilize the active configuration of the voltage sensor by modifying the equilibrium constant between voltage sensor resting and active states *and* slows down the opening and closing kinetics by increasing the energy barrier between the intermediate closed states and the open states. Intermediate closed states are consistent with the closing of secondary gates and, as we discuss below, there are previous reports of their existence.

In the absence of Ca^{2+}, a voltage gating scheme based on an allosteric mechanism could approximate the basic features of the voltage dependence of BK channels. This mechanism results in a gating scheme (Fig. S5*A*) that contains a parallel arrangement of open and closed states (24, 25). However, there is evidence that, although the allosteric model can account for the effects of voltage and Ca^{2+} on the open probability of BK channels composed only of α subunits, it cannot account for the detailed single channel kinetics (33).Cox et al. (33) suggested that additional states are needed. The detailed single-channel kinetic analysis performed by Rothberg and Magleby (34; see also ref. 35) confirmed this prediction. They found that minimal models able to account for the kinetic structure of BK channels require additional brief closed states, either in the activation pathway or beyond the activation pathway as secondary states. A three-tiered kinetic scheme with two rows of closed estates was also used by Zeng et al. (36) to explain the double Boltzmann shape of the *G–V* curves of (α/β3)BK channels. We propose here that β1, β2, and β4 subunits make apparent the existence of such closed states in the activation pathway as intermediate states.

Although most studies indicate that the β1 and β2 subunits increase Ca^{2+} sensitivity through different mechanisms, it is at present unclear whether or not β2 subunits affect the voltage sensor functioning (18, 20, 30). Using the voltage clamp fluorometry technique, Savalli et al. (30) found that the (α/β2)BK fluorescence–voltage $F(V)$ curves were left shifted with respect to the (α)BK *F–V* relationship, strongly suggesting that, as is the case of the β1 subunit, β2 favor the activated conformation of the BK voltage sensor. On the other hand, mutations that perturb the voltage sensor equilibrium between resting and active configuration or the number of equivalent gating charges disrupt the ability of β1 to increase the Ca^{2+} sensitivity but not that of β2 (21). Therefore, contrary to what was concluded by Savalli et al. (30) Yang et al. (21) results indicate that β2 and β1 functions are governed by different mechanisms. Actually, it has been proposed that the β2 subunit mainly modulates the coupling between Ca^{2+} binding and channel opening (29). Here, using gating current recordings we found that β2 stabilizes the active configuration of the voltage sensor, albeit to a lesser extent ($\Delta V_{1/2}$ = −40 mV) than the β1 subunit (Fig. 2*B*) and it does not affect the gating charge on the voltage sensor of the BK channel. This is a unique direct demonstration that β2 is modifying the Ca^{2+} sensitivity of BK channels through a mechanism that also involves a stabilization of the active configuration of the voltage sensor.

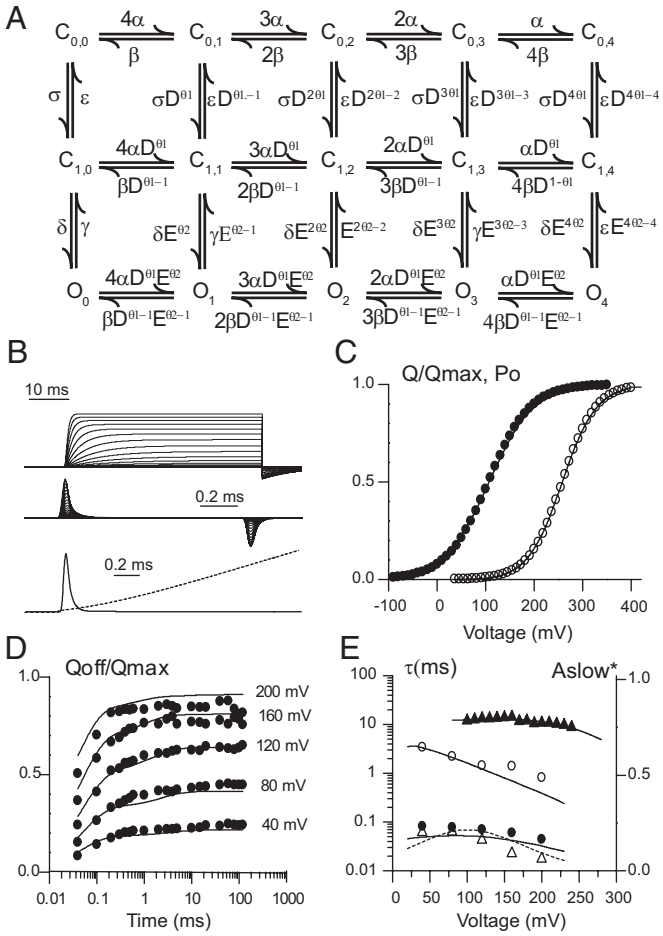

Fig. 4. Allosteric model in which the channel gate opens in two sequential steps. (*A*) Diagram showing in each row the states corresponding to the different combination of the four voltage sensors either in the resting or active position with voltage-dependent rates $\alpha(V)$ and $\beta(V)$. Columns depict a single gate that opens in two steps; the first governed by rates σ and ε connect to an intermediate closed state that then opens and closes with rates δ and γ, respectively. With the activation of each voltage sensor these transitions are favored by allosteric constant *D* and *E*. These allosteric constants will influence the forward rate by a fraction θ, whereas the backward rates by $\theta-1$. (*B*) Simulated I_K and I_g current experiments using this model with the following parameters: $\alpha = 1{,}880\ s^{-1}$, $\beta = 21{,}500\ s^{-1}$ with $z_\alpha = 0.49$ and $\delta_\alpha = 0.63$. Transition rates between $C_{0,i}$ and $C_{1,i}$ were $\sigma = 50.4\ s^{-1}$ and $\varepsilon = 205\ s^{-1}$ with z_ε and δ_ε set to 0. *D* was 2.75 with $\theta = 0.94$ and $\delta = 0.9\ s^{-1}$ and $\gamma = 318$, $z_\delta = 0.604$ and $\delta_\delta = 0.726$. Allosteric constant *E* was set to 1. Top traces correspond to simulated ionic current (*Upper*) and gating current traces during depolarizing steps of increasing amplitude. A 50-ms pulse from −90 mV that sweeps from +20 to 350 mV in 20 mV increments was used to simulate I_K, whereas a 1-ms pulse spanning from −80 to 300 mV was preferred for I_g. Superimposed gating I_g (solid line) and I_K (dashed line) at the beginning of a depolarizing pulse to +200 mV is shown (*Lower*). (*C*) Simulated *Q–V* and P_o together with experimental data from (α/β1) BK channels. *Q–V* were obtained by integrating the first 500 μs of the simulated I_g at the end of the pulse. P_o was obtained by normalizing the simulated current amplitudes at the end of a 120-ms pulse. Closed circles correspond to the experimental data described in Fig. 2*C*, whereas open circles correspond to normalized *G–V* (from ref. 33). (*D*) Fast and slow charge movement measured during repolarization to −90 mV following a depolarizing pulse of different durations and voltages. (*E*) Voltage dependence of the time constants of Q_{OFF} and I_K in *D* and *E*; symbols correspond to data described in Fig. 3 and continuous line from simulated I_g at the same voltages and durations.

Regarding, the effects of β3b, changes in channel gating even when the N terminus is removed have been detected (36). In particular, the voltage dependence of activation exhibits multiple Boltzmann components. Our results indicate that, if the β3b makes more prominent the independent voltage-dependent transitions that participate in BK channel activation, these are not reflected in closed–closed voltage-dependent transitions. It is possible that β3b modifies the kinetics or the equilibrium of the open–open and closed–open transitions. An analysis of (α/β4)BK single channel and macroscopic current records using the allosteric model suggested that it was possible to explain the effects of β4 by a decrease in the equilibrium constant describing the closed–open equilibrium (L_0) and a shift to the left of the *Q–V* relationship (17). The present results show that β4 stabilizes the active conformation of the voltage sensor and that the number of gating charges per sensor is decreased. These finding are sufficient to explain the changes in BK channel Ca^{2+} sensitivity induced by β4 (Fig. S6). However, the behavior of Q_{slow} in (α/β4)BK channels suggest that the three-tiered model we proposed here should be more appropriate to fully account for the modulation in BK channel gating induced by β4.

Materials and Methods

Channel Expression. BK α subunit (U11058), human β subunit's 1 and 4 (U25138 and AF160967), and β2 subunit (AF099137) without inactivation domain (β2IR) (6) were provided by L. Toro (University of California, Los Angeles, CA). β3b (AF160968) subunit was provided by C. Lingle (University of Washington, St. Louis, MO). mMESSAGE mMACHINE (Ambion) was used for in vitro transcription. *Xenopus* oocytes were injected with ∼40 ng of α subunit cRNA, or a mixture of ∼40 ng (α subunit) and ∼100 ng (β subunit) was injected per oocyte, 4–8 d before recording. The approximate RNA molar ratio β:α was at least 3:1, ensuring saturation of the α subunits with β subunit.

Electrophysiology. Using the patch-clamp technique, ionic currents (I_k) were recorded in the cell-attached mode and gating currents (I_g) in the inside-out configuration. The internal solution contained (in millimoles) 110 *N*-methyl-D-glucamine (NMDG)–$MeSO_3$, 10 Hepes and 5 EGTA, reducing free [Ca] nearly to an estimated 0.8 nM based on the presence of ∼10 μM contaminant Ca^{2+} (33). The external (pipette) solution contained 110 tetraethylammonium (TEA)–$MeSO_3$, 10 Hepes, 2 $MgCl_2$; pH was adjusted to 7. Experiments were performed at room temperature (20–22 °C). I_K currents were recorded in cell-attached mode using the internal K^+ of the oocyte. To measure gating currents in the same oocyte, the patch was excised and washed with internal solution, at least 10–20 times the volume of the chamber.

Pipettes of borosilicate capillary glass (Corning; 7740, Pyrex) were pulled in a horizontal pipette puller (Sutter Instruments). Pipette resistance was 100–400 kΩ (20–60 μm), after fire polished. Data were acquired with an Axopatch 200B (Axon Instruments) amplifier. Both the voltage command and current output were filtered at 20 kHz with 8-pole Bessel low-pass filter (Frequency Devices). Current signals were sampled with a 16-bit A/D converter (Digidata 1322A; Axon Instruments), using a sampling rate of 500 kHz. Experiments were performed using Clampex 8 (Axon Instruments) acquisition software. Leak subtraction was performed using a P/4 protocol (37).

Data Analysis. All data analysis was performed using Clampfit 10 (Axon Instruments) and Excel 2007 (Microsoft). Gating currents were integrated between 0 and 400 μs after the voltage step to obtain the net charge movement. Leakage current was subtracted by shifting the current until the integral no longer changed after 1 ms after the voltage step. *Q–V* relation was fitted with a Boltzmann function: $Q = Q_{max}/(1-\exp(-zF(V-V_h)/RT))$, where Q_{max} is the maximum charge, *z* is the voltage dependency of activation, V_h is the half-activation voltage, *T* is the absolute temperature (typically 295 K), *F* is the Faraday's constant, and *R* is the universal gas constant. Q_{max}, V_h, and *z* were determined using Solver complement of Microsoft Excel. The OFF charge determined as a function of the duration of the ON pulse, Q_p, was fitted with a two-exponential function:

$$Q_p = Q_{fast}\left(1-\exp\left(-t/\tau_{fast}\right)\right) + Q_{slow}\left(1-\exp\left(-t/\tau_{slow}\right)\right),$$

where *t* is the duration of the ON pulse, Q_{fast}, Q_{slow}, τ_{fast}, and τ_{slow} are the charges and the time constants of the slow and fast charge movement kinetics, respectively. These values were determined using least square minimization.

Simulations of Gating and Ionic Currents. BK channel gating and ionic current were simulated on Matlab (MathWorks) by solving the time dependencies of the distribution of states ($S(t)$) during a voltage pulse protocol by calculating:

$\vec{S}(t) = \vec{S}(0) \cdot \exp(Q \cdot t)$, where Q is the standard rate matrix as described in Colquhoun and Hawk (38). Using the spectral decomposition method, we obtained the time constants and amplitudes that describe the relaxation of a multistate system. The time course of I_K and I_g can then be calculated from:

$$I_K(t) = S_j = N \cdot \vec{S}(t) \cdot \vec{G}$$

$$I_g(t) = N \cdot \vec{S}(t) \cdot \vec{F}.$$

N is the number of channel and G is a vector containing the single-channel conductance for each state. F is a vector in which each element corresponds to the net flux of charges involved in leaving each state. These were obtained by multiplying the rate of each transition by the charges displaced in that transition (39).

All simulations were carried out using a sampling rate of 500 kHz and digitally filtered at 20 KHz with a numerical implementation of an 8-pole Bessel filter. Total charge displaced at the end of a pulse (Q_{off}) was obtained by integrating 500 μs of simulated I_g. The channel apparent Po was obtained from $I_K(t)$ at the end of a 120-ms pulse. The set of parameters p_k defining the model that described the data were obtained by minimizing the cost function $SSQ(p_k)$ with a "simplex" algorithm Nelder and Mead (40).

$$SSQ(p_k) = \sum_j A_j \left[\sum_i (f_i - x_i)^2 / n\max(x_i) \right].$$

The relative error of each individual type of experiment was scaled by an arbitrary factor (A_j) and normalized by the number of data point (n) times the maximum of each particular data set (max(xi)).

ACKNOWLEDGMENTS. We thank Dr. Enrico Stefani for teaching us all the experimental secrets involved in the gating current measurements and Luisa Soto for excellent technical assistance. This work was supported by FONDECYT Grants 1110430 (to R.L.), 1120802 (to C.G.), and 1120864 (to A.N.); ANILLO Grant ACT1104 (to C.G. and A.N.); the Chile–Argentina exchange grant 2011-665 CH/11/12 (to R.L. and C.G.); CONICYT doctoral fellowships (to G.F.C.); and Doctoral Thesis Support Fellowship AT-24110157 (to G.F.C.). The Centro Interdisciplinario de Neurociencia de Valparaíso is a Millennium Institute supported by the Millennium Scientific Initiative of the Ministerio de Economía, Fomento y Turismo.

1. Marty A (1981) Ca-dependent K channels with large unitary conductance in chromaffin cell membranes. *Nature* 291(5815):497–500.
2. Pallotta BS, Magleby KL, Barrett JN (1981) Single channel recordings of Ca2+-activated K+ currents in rat muscle cell culture. *Nature* 293(5832):471–474.
3. Latorre R, Vergara C, Hidalgo C (1982) Reconstitution in planar lipid bilayers of a Ca2+-dependent K+ channel from transverse tubule membranes isolated from rabbit skeletal muscle. *Proc Natl Acad Sci USA* 79(3):805–809.
4. Orio P, Rojas P, Ferreira G, Latorre R (2002) New disguises for an old channel: MaxiK channel beta-subunits. *News Physiol Sci* 17:156–161.
5. Knaus HG, et al. (1994) Primary sequence and immunological characterization of beta-subunit of high conductance Ca(2+)-activated K+ channel from smooth muscle. *J Biol Chem* 269(25):17274–17278.
6. Wallner M, Meera P, Toro L (1999) Molecular basis of fast inactivation in voltage and Ca2+-activated K+ channels: A transmembrane beta-subunit homolog. *Proc Natl Acad Sci USA* 96(7):4137–4142.
7. Behrens R, et al. (2000) hKCNMB3 and hKCNMB4, cloning and characterization of two members of the large-conductance calcium-activated potassium channel beta subunit family. *FEBS Lett* 474(1):99–106.
8. Brenner R, Jegla TJ, Wickenden A, Liu Y, Aldrich RW (2000) Cloning and functional characterization of novel large conductance calcium-activated potassium channel beta subunits, hKCNMB3 and hKCNMB4. *J Biol Chem* 275(9):6453–6461.
9. Meera P, Wallner M, Toro L (2000) A neuronal beta subunit (KCNMB4) makes the large conductance, voltage- and Ca2+-activated K+ channel resistant to charybdotoxin and iberiotoxin. *Proc Natl Acad Sci USA* 97(10):5562–5567.
10. Uebele VN, et al. (2000) Cloning and functional expression of two families of beta-subunits of the large conductance calcium-activated K+ channel. *J Biol Chem* 275(30): 23211–23218.
11. Xia XM, Ding JP, Lingle CJ (1999) Molecular basis for the inactivation of Ca2+- and voltage-dependent BK channels in adrenal chromaffin cells and rat insulinoma tumor cells. *J Neurosci* 19(13):5255–5264.
12. Chen M, et al. (2008) Lysine-rich extracellular rings formed by hbeta2 subunits confer the outward rectification of BK channels. *PLoS ONE* 3(5):e2114.
13. Xia XM, Ding JP, Zeng XH, Duan KL, Lingle CJ (2000) Rectification and rapid activation at low Ca2+ of Ca2+-activated, voltage-dependent BK currents: Consequences of rapid inactivation by a novel beta subunit. *J Neurosci* 20(13):4890–4903.
14. Zeng XH, Xia XM, Lingle CJ (2003) Redox-sensitive extracellular gates formed by auxiliary beta subunits of calcium-activated potassium channels. *Nat Struct Biol* 10(6): 448–454.
15. Ha TS, Heo MS, Park CS (2004) Functional effects of auxiliary beta4-subunit on rat large-conductance Ca(2+)-activated K(+) channel. *Biophys J* 86(5):2871–2882.
16. Wang B, Brenner R (2006) An S6 mutation in BK channels reveals beta1 subunit effects on intrinsic and voltage-dependent gating. *J Gen Physiol* 128(6):731–744.
17. Wang B, Rothberg BS, Brenner R (2006) Mechanism of beta4 subunit modulation of BK channels. *J Gen Physiol* 127(4):449–465.
18. Lee US, Cui J (2009) Beta subunit-specific modulations of BK channel function by a mutation associated with epilepsy and dyskinesia. *J Physiol* 587(Pt 7):1481–1498.
19. Bao L, Cox DH (2005) Gating and ionic currents reveal how the BKCa channel's Ca2+ sensitivity is enhanced by its beta1 subunit. *J Gen Physiol* 126(4):393–412.
20. Orio P, Latorre R (2005) Differential effects of beta 1 and beta 2 subunits on BK channel activity. *J Gen Physiol* 125(4):395–411.
21. Yang H, et al. (2008) Subunit-specific effect of the voltage sensor domain on Ca2+ sensitivity of BK channels. *Biophys J* 94(12):4678–4687.
22. Sweet TB, Cox DH (2009) Measuring the influence of the BKCa beta1 subunit on Ca2+ binding to the BKCa channel. *J Gen Physiol* 133(2):139–150.
23. Lee US, Cui J (2010) BK channel activation: Structural and functional insights. *Trends Neurosci* 33(9):415–423.
24. Horrigan FT, Cui J, Aldrich RW (1999) Allosteric voltage gating of potassium channels I. Mslo ionic currents in the absence of Ca(2+). *J Gen Physiol* 114(2):277–304.
25. Horrigan FT, Aldrich RW (1999) Allosteric voltage gating of potassium channels II. Mslo channel gating charge movement in the absence of Ca(2+). *J Gen Physiol* 114(2): 305–336.
26. Stefani E, et al. (1997) Voltage-controlled gating in a large conductance Ca2+-sensitive K+channel (hslo). *Proc Natl Acad Sci USA* 94(10):5427–5431.
27. Horrigan FT, Aldrich RW (2002) Coupling between voltage sensor activation, Ca2+ binding and channel opening in large conductance (BK) potassium channels. *J Gen Physiol* 120(3):267–305.
28. Nimigean CM, Magleby KL (2000) Functional coupling of the beta(1) subunit to the large conductance Ca(2+)-activated K(+) channel in the absence of Ca(2+). Increased Ca(2+) sensitivity from a Ca(2+)-independent mechanism. *J Gen Physiol* 115(6):719–736.
29. Lee US, Shi J, Cui J (2010) Modulation of BK channel gating by the ß2 subunit involves both membrane-spanning and cytoplasmic domains of Slo1. *J Neurosci* 30(48): 16170–16179.
30. Savalli N, Kondratiev A, de Quintana SB, Toro L, Olcese R (2007) Modes of operation of the BKCa channel beta2 subunit. *J Gen Physiol* 130(1):117–131.
31. Cox DH, Aldrich RW (2000) Role of the beta1 subunit in large-conductance Ca(2+)-activated K(+) channel gating energetics. Mechanisms of enhanced Ca(2+) sensitivity. *J Gen Physiol* 116(3):411–432.
32. Qian X, Magleby KL (2003) Beta1 subunits facilitate gating of BK channels by acting through the Ca2+, but not the Mg2+, activating mechanisms. *Proc Natl Acad Sci USA* 100(17):10061–10066.
33. Cox DH, Cui J, Aldrich RW (1997) Separation of gating properties from permeation and block in mslo large conductance Ca-activated K+ channels. *J Gen Physiol* 109(5): 633–646.
34. Rothberg BS, Magleby KL (1998) Kinetic structure of large-conductance Ca2+-activated K+ channels suggests that the gating includes transitions through intermediate or secondary states. A mechanism for flickers. *J Gen Physiol* 111(6):751–780.
35. Shelley C, Niu X, Geng Y, Magleby KL (2010) Coupling and cooperativity in voltage activation of a limited-state BK channel gating in saturating Ca2+. *J Gen Physiol* 135 (5):461–480.
36. Zeng XH, Ding JP, Xia XM, Lingle CJ (2001) Gating properties conferred on BK channels by the beta3b auxiliary subunit in the absence of its NH(2)- and COOH termini. *J Gen Physiol* 117(6):607–628.
37. Armstrong CM, Bezanilla F (1973) Currents related to movement of the gating particles of the sodium channels. *Nature* 242(5398):459–461.
38. Colquhoun D, Hawkes AG (1982) On the stochastic properties of bursts of single ion channel openings and of clusters of bursts. *Philos Trans R Soc Lond B Biol Sci* 300 (1098):1–59.
39. Santiago-Castillo JA, Covarrubias M, Sánchez-Rodríguez JE, Perez-Cornejo P, Arreola J (2010) Simulating complex ion channel kinetics with IonChannelLab. *Channels (Austin)* 4(5):422–428.
40. Nelder JA, Mead R (1965) A simplex method for function minimization. *Comput J* 7(4): 308–313.